An irradiated brown dwarf companion to an accreting white dwarf

Juan V. Hernández Santisteban[1], Christian Knigge[1], Stuart P. Littlefair[2], Rene P. Breton[3,1], Vik S. Dhillon[2,4], Boris T. Gänsicke[5], Thomas R. Marsh[5], Magaretha L. Pretorius[6], John Southworth[7] & Peter H. Hauschildt[8]

[1]*Department of Physics and Astronomy, University of Southampton, Southampton SO17 1BJ, UK*

[2]*Department of Physics and Astronomy, University of Sheffield, S3 7RH, UK*

[3]*The School of Physics and Astronomy, The University of Manchester, Manchester, UK*

[4]*Instituto de Astrofísica de Canarias, E-38205 La Laguna, Santa Cruz de Tenerife, Spain*

[5]*Department of Physics, University of Warwick, Coventry CV4 7AL, UK*

[6]*Department of Physics, University of Oxford, Denys Wilkinson Building, Keble Road, OX1 3RH, Oxford, UK*

[7]*Astrophysics Group, Keele University, Staffordshire, ST5 5BG, UK*

[8]*Hamburger Sternwarte, Gojenbergsweg 112, 21029 Hamburg, Germany*

Brown dwarfs and giant planets orbiting close to a host star are subjected to significant irradiation that can modify the properties of their atmospheres. In order to test the atmospheric models that are used to describe these systems, it is necessary to obtain accurate observational estimates of their physical properties (masses, radii, temperatures, albedos). Interacting compact binary systems provide a natural laboratory for studying strongly irradiated sub-stellar objects. As the mass-losing secondary in these systems makes a crit-

ical, but poorly understood transition from the stellar to the sub-stellar regime, it is also strongly irradiated by the compact accretor[1,2]. In fact, the internal and external energy fluxes are both expected to be comparable in these objects, providing access to an unexplored irradiation regime. However, the atmospheric properties of such donors have so far remained largely unknown[3]. Here, we report the direct spectroscopic detection and characterisation of an irradiated sub-stellar donor in an accreting white dwarf binary system. Our near-infrared observations allow us to determine a model-independent mass estimate for the donor of $M_2 = 0.055 \pm 0.008 M_\odot$ and an average spectral type of $\mathrm{L1} \pm 1$, supporting both theoretical predictions and model-dependent observational constraints. Our time-resolved data also allow us to estimate the average irradiation-induced temperature difference between the day and night sides on the sub-stellar donor, $\Delta \mathrm{T} \simeq 57$ K, and the maximum difference between the hottest and coolest parts of its surface, of $\Delta \mathrm{T}_{max} \simeq 200$ K. The observations are well described by a simple geometric reprocessing model with a bolometric (Bond) albedo of $A_B < 0.54$ at the 2-σ confidence level, consistent with high reprocessing efficiency, but poor lateral heat redistribution in the donor's atmosphere[4,5].

Only a single brown dwarf donor to an accreting white dwarf has been detected spectroscopically to date[3], and no empirical information at all is available regarding the effect of irradiation on the donor's atmosphere. We have therefore carried out simultaneous optical and near-infrared time-resolved spectroscopy of one such system with the X-Shooter instrument[6] at the Very Large Telescope (ESO). Our target, SDSS J143317.78+101123.3[7] (J1433 hereafter), is an eclipsing system with a short orbital period ($P_{orb} = 78.1$ min) and a likely donor mass well below the

hydrogen-burning limit, as estimated from eclipse modelling ($M_2 = 0.0571 \pm 0.0007 M_\odot$[8,9]). The exceptionally wide wavelength coverage provided by our data set (0.35 μm - 2.5 μm) allows us to confidently dissect the overall spectral energy distribution. This is illustrated in Fig. 1. Disk-formed, double-peaked hydrogen emission lines can be seen across the entire spectral range. The presence of broad Balmer absorption lines between 0.3 μm and 0.5 μm shows that the white dwarf is the strongest emitter in this wave band. However, the donor star spectrum is clearly visible in the near-infrared and dominates between 1.0 μm and 2.5 μm.

The clear donor signature in the near-infrared allows us to isolate the donor's spectrum and determine its properties. We decomposed the average spectrum by fitting the optical region with a white dwarf atmosphere model[10] and an accretion disc (modelled as a simple power law). Both of these contributions were then extrapolated to the near-infrared and subtracted in order to retrieve a pure donor spectrum. This donor spectrum was then compared to an empirical brown dwarf spectral sequence[11]. The best-matching spectral type was found to be SpT=L1$\pm$1, which agrees remarkably well with semi-empirical evolutionary predictions[1,2] and with previous narrow J-band estimates[3].

These results imply that the donor in J1433 has successfully undergone the transition from the stellar to the sub-stellar regime. The alternative – that the secondary was born as a brown dwarf – is extremely unlikely. First, extreme mass-ratio binary systems containing very low mass objects ($M \lesssim 0.1$ M$_\odot$) are intrinsically rare [12]. Second, the mass of the accreting white dwarf in J1433, M$_{WD} = 0.80 \pm 0.07$ M$_\odot$, is exactly in line with the mean white dwarf mass of known accreting

white dwarf systems going through the standard evolution channel[13], but significantly higher than the average mass of isolated white dwarfs ($\langle \mathrm{M}_{WD} \rangle \simeq 0.6\,\mathrm{M}_{\odot}$[13]) and that of any known primary in a white dwarf-brown dwarf binary system[14]. Third, the orbital period of J1433 lies squarely within the "period minimum spike" that coincides with the stellar to sub-stellar transition of the donor star in systems born with main-sequence companions[15]. By contrast, systems born with sub-stellar donors would be expected to populate a wide range of orbital periods below this spike[16]. However, no such systems have ever been found. Indeed, the only accreting white dwarf with a sub-stellar donor and an orbital period well below P_{min} has been shown to be a low-metallicity object in the Galactic halo[17], rather than a system born with a brown dwarf secondary.

Models of irradiated planets suggest that irradiation can increase photospheric temperatures by an order of magnitude compared to an isolated object, with significant effects on the planet's radius and atmospheric structure[18]. Furthermore, a long-standing mismatch between the predicted and observed minimum period for accreting white dwarf binary systems can be traced to a $\sim 10\%$ offset between the donor radii inferred from observations and those predicted by theoretical model atmospheres[19]. However, such large effects are only possible if the irradiating flux is efficiently absorbed in the atmosphere and redistributed across the terminator, i.e. from the day-side to the night-side[2,20]. This is necessary since it is the blocking effect of the incoming radiation on the outward heat flux from the secondary's interior that drives the irradiation-induced swelling of the donor.

Globally, the bolometric flux emitted by the irradiated donor must always balance the sum of

its intrinsic flux and the irradiation flux it has absorbed[21]. However, in the absence of redistribution, this balance must be maintained locally in the atmosphere. This should produce pronounced temperature differences between the day- and night-sides on the tidally-locked donor. Since the system is seen close to edge-on, such differences should manifest as changes in the apparent spectral type of the donor as a function of orbital phase. We have tested for this by measuring the H_2O 1.3 μm band index[11]. Water vapour is the most sensitive absorber in irradiated hot Jupiters[22], and water band strength has been shown to correlate well with spectral type and effective temperature[11]. As shown in Fig. 2b, we detect a spectroscopic change of ΔSpT$\simeq$ 1 (i.e. M9-L0), with a maximum at phase 0.5, precisely where the day-side of the donor is exposed.

On its own, this spectroscopic signal would be only marginally significant, as a model without irradiation can be ruled out at only a 2σ confidence level. However, an independent irradiation signature is provided by the observed broad-band flux variations around the orbit, which are shown in Fig. 2c. This figure reveals a double modulation over one orbit, which is produced by the combination of two effects: the distorted shape of the tidally-locked, Roche-lobe-filling donor star (ellipsoidal variations) and the temperature difference between its day- and night-side (irradiation effect). In order to quantify the irradiation effect, we used the binary light curve synthesis code ICARUS[23] to fit both the water-band and broad-band modulations under the assumption of no heat redistribution between hemispheres. As shown in Fig. 2, the resulting fit is acceptable and provides a plausible representation of the temperature distribution across the surface of the donor. The average temperature of the day-side is $\langle T_{day} \rangle = 2401 \pm 10$ K, and a night-side temperature of $\langle T_{night} \rangle = 2344 \pm 7$ K. These numbers are consistent with the mean donor temperature obtained

from the template-calibrated spectral type measurements.

The observed difference between the day-side and night-side fluxes is statistically significant and allows us to estimate the reprocessing efficiency of the donor. This efficiency is usually parametrised via the bolometric (Bond) albedo, A_B, which is the fraction of the incident irradiation flux that is not reprocessed, but reflected back into space. The irradiating source in the system is the hot white dwarf. We therefore obtained an improved measurement of its temperature, $T_{WD} = 13,200 \pm 200$ K, by making use of ultraviolet observations obtained by the GALEX satellite. With this, we find $A_B < 0.54$ at 2-σ confidence, as shown in Extended Figure 1. This low value implies a high reprocessing efficiency in the atmosphere of the donor. We can also use the observed difference between day-side and night-side fluxes to estimate the efficiency with which radiation absorbed locally is redistributed across the donor, ϵ (see Methods). We find a limit for the redistribution efficiency of $\epsilon < 0.54$ at 2-σ confidence. Efficient reprocessing, coupled with poor heat redistribution, has also been found in hot Jupiters in this atmospheric temperature regime [5] and suggested for low-mass stars in accreting white dwarfs[4]. If irradiation is the main cause of the larger-than-predicted donor radii[19], efficient heat redistribution is required. Our finding that day-side to night-side heat transfer must be modest therefore suggests that irradiation is unlikely to be responsible for inflating the donors. Instead, the dominant effect of irradiation is simply an increase in the local temperature[4].

In most hot Jupiters, the external irradiation overwhelms any internal heat flux. The relatively milder irradiation experienced by the donor in J1433, coupled with the unique prospect of obtaining

detailed phase-resolved spectra and line profiles, will permit quantitative tests of irradiated model atmospheres in a regime where these observables are expected to be quite sensitive to irradiation. The system also provides an independent new benchmark for theoretical models that predict the albedo and heat redistribution efficiency in irradiated planetary atmospheres [5]. Finally, the donor in J1433 is a rapid rotator ($v \sin i = 131 \pm 46$ km s^{-1}), which could have interesting and significant effects on its atmospheric dynamics[24].

1. Knigge, C. The donor stars of cataclysmic variables. *Mon. Not. R. Astron. Soc* **373**, 484–502 (2006).

2. Knigge, C., Baraffe, I. & Patterson, J. The Evolution of Cataclysmic Variables as Revealed by Their Donor Stars. *ApJS* **194**, 28 (2011).

3. Littlefair, S. P. *et al.* A J-band detection of the sub-stellar mass donor in SDSS J1433+1011. *Mon. Not. R. Astron. Soc* **431**, 2820–2825 (2013).

4. Barman, T. S., Hauschildt, P. H. & Allard, F. Model Atmospheres for Irradiated Stars in Precataclysmic Variables. *Astrophys. J.* **614**, 338–348 (2004).

5. Perez-Becker, D. & Showman, A. P. Atmospheric Heat Redistribution on Hot Jupiters. *Astrophys. J.* **776**, 134 (2013).

6. Vernet, J. *et al.* X-shooter, the new wide band intermediate resolution spectrograph at the ESO Very Large Telescope. *Astron. Astrophys.* **536**, A105 (2011).

7. Szkody, P. *et al.* Cataclysmic Variables from Sloan Digital Sky Survey. VI. The Sixth Year (2005). *Astron. J.* **134**, 185–194 (2007).

8. Littlefair, S. P. *et al.* A Brown Dwarf Mass Donor in an Accreting Binary. *Science* **314**, 1578– (2006).

9. Savoury, C. D. J. *et al.* Cataclysmic variables below the period gap: mass determinations of 14 eclipsing systems. *Mon. Not. R. Astron. Soc* **415**, 2025–2041 (2011).

10. Hubeny, I. & Lanz, T. Non-LTE line-blanketed model atmospheres of hot stars. 1: Hybrid complete linearization/accelerated lambda iteration method. *Astrophys. J.* **439**, 875–904 (1995).

11. Cushing, M. C., Rayner, J. T. & Vacca, W. D. An Infrared Spectroscopic Sequence of M, L, and T Dwarfs. *Astrophys. J.* **623**, 1115–1140 (2005).

12. Burgasser, A. J. *et al.* Not Alone: Tracing the Origins of Very-Low-Mass Stars and Brown Dwarfs Through Multiplicity Studies. *Protostars and Planets V* 427–441 (2007).

13. Zorotovic, M., Schreiber, M. R. & Gänsicke, B. T. Post common envelope binaries from SDSS. XI. The white dwarf mass distributions of CVs and pre-CVs. *Astron. Astrophys.* **536**, A42 (2011).

14. Nordhaus, J. & Spiegel, D. S. On the orbits of low-mass companions to white dwarfs and the fates of the known exoplanets. *Mon. Not. R. Astron. Soc* **432**, 500–505 (2013).

15. Gänsicke, B. T. & Koester, D. SW Ursae Majoris, CU Velorum and AH Mensae: three more accreting white dwarfs unveiled? *Astron. Astrophys.* **346**, 151–157 (1999).

16. Politano, M. The Formation of Cataclysmic Variables with Brown Dwarf Secondaries. *Astrophys. J.* **604**, 817–826 (2004).

17. Uthas, H., Knigge, C., Long, K. S., Patterson, J. & Thorstensen, J. The cataclysmic variable SDSS J1507+52: an eclipsing period bouncer in the Galactic halo. *Mon. Not. R. Astron. Soc* **414**, L85–L89 (2011).

18. Arras, P. & Bildsten, L. Thermal Structure and Radius Evolution of Irradiated Gas Giant Planets. *Astrophys. J.* **650**, 394–407 (2006).

19. Littlefair, S. P. *et al.* On the evolutionary status of short-period cataclysmic variables. *Mon. Not. R. Astron. Soc* **388**, 1582–1594 (2008).

20. Ritter, H., Zhang, Z.-Y. & Kolb, U. Irradiation and mass transfer in low-mass compact binaries. *Astron. Astrophys.* **360**, 969 (2000).

21. Ruciński, S. M. The Proximity Effects in Close Binary Systems. II. The Bolometric Reflection Effect for Stars with Deep Convective Envelopes. *Acta Astronomica* **19**, 245 (1969).

22. Stevenson, K. B. *et al.* Thermal structure of an exoplanet atmosphere from phase-resolved emission spectroscopy. *Science* **346**, 838–841 (2014).

23. Breton, R. P., Rappaport, S. A., van Kerkwijk, M. H. & Carter, J. A. KOI 1224: A Fourth Bloated Hot White Dwarf Companion Found with Kepler. *Astrophys. J.* **748**, 115 (2012).

24. Showman, A. P. & Kaspi, Y. Atmospheric Dynamics of Brown Dwarfs and Directly Imaged Giant Planets. *Astrophys. J.* **776**, 85 (2013).

Acknowledgements Based on observations made with ESO Telescopes at the La Silla Paranal Observatory under programme ID 085.D-0489. J.V.H.S acknowledges support via studentships from CONACyT (Mexico) and the University of Southampton, as well as research support by the Royal Astronomical Society. R.P.B. has received funding from the European Union eleventh Framework Programme under grant agreement PIIF-GA-2012-332393. BTG was supported by ERC Grant Agreement n. 320964.

Author Contributions C.K., S.P.L., V.S.D, B.T.G, T.R.M, M.L.P. and J.S proposed and planned the observations. All data analysis was done by J.V.H.S with significant feedback from C.K., R.P.B. and S.P.L. All authors discussed the results and commented on the manuscript.

Author Information Correspondence and requests for materials should be addressed to J.V.H.S. (email: j.v.hernandez@soton.ac.uk).

Competing Interests The authors declare that they have no competing financial interests.

Code Availability. The code used to generate the model, as well as the atmosphere templates, ICARUS, is available at https://github.com/bretonr/Icarus.

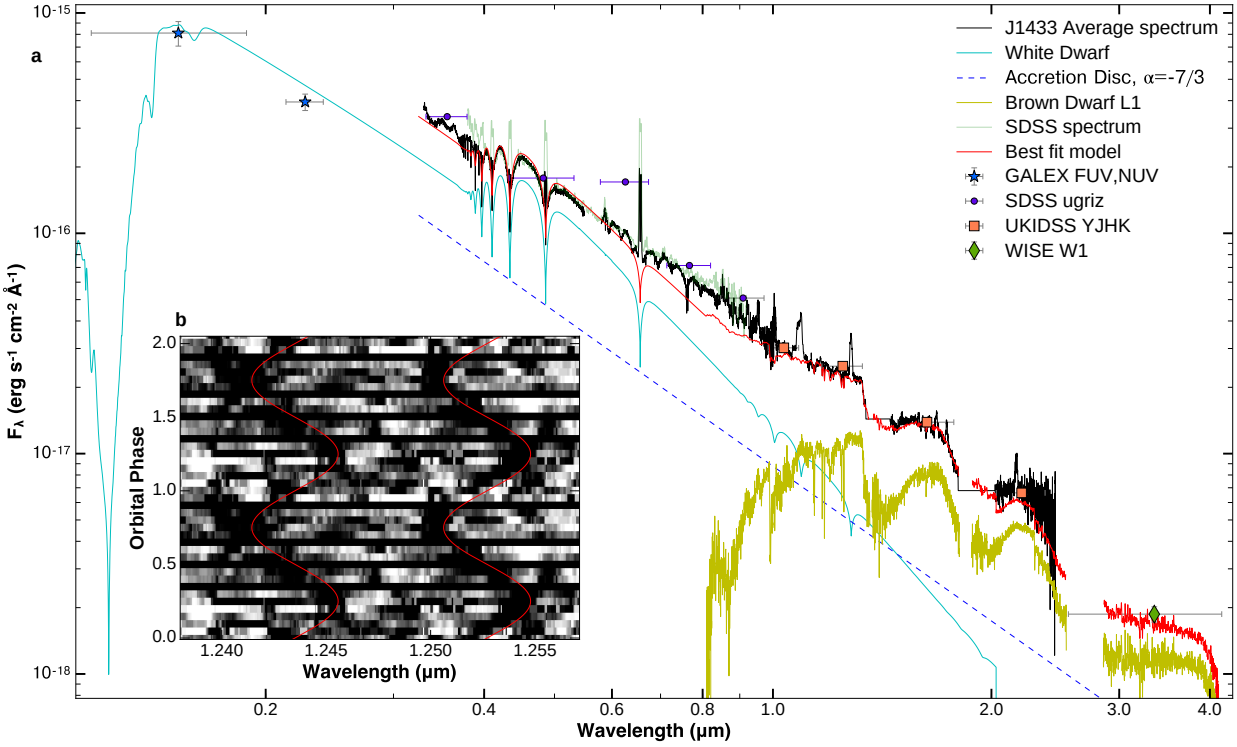

Figure 1 | The average optical and near-infrared spectral energy distribution of SDSS J143317.78+101123.3. **a**, The overall fit to the spectra using a white dwarf atmosphere model and brown dwarf templates was performed. The accretion disc contribution was described as a simple power law. We obtained a best fit with a spectral type of L1$\pm$1. SDSS, UKIDSS and WISE photometry are shown for reference. **b**, Trailed, phase-binned spectra around the K I doublet at 1.2436 μm and 1.2528 μm. These features arise in the atmosphere of the donor star, enabling the determination of orbital parameters such as the semi-amplitude $K_2 = 499 \pm 15$ km s^{-1}, the rotational broadening of the donor $v \sin i = 131 \pm 46$ km s^{-1} and systemic velocity $\gamma = -42 \pm 8$ km s^{-1}.

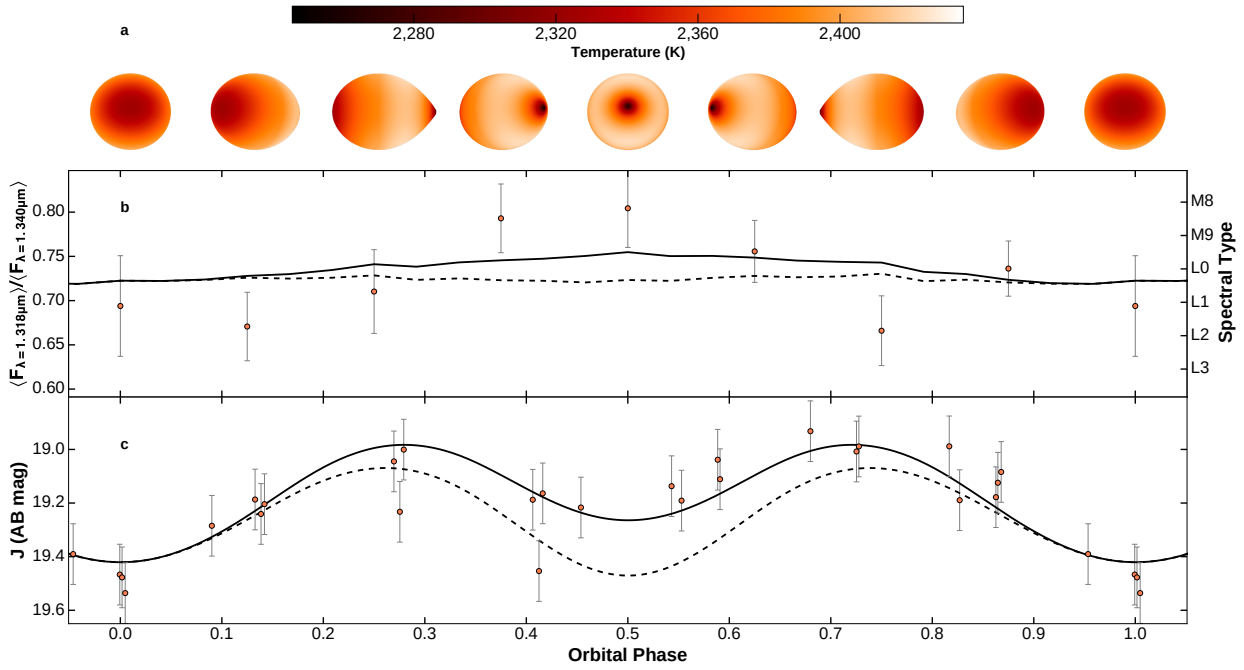

Figure 2 | Ellipsoidal and irradiation effects associated with the substellar donor in SDSS J143317.78+101123.3. We find a difference in spectral type between the day-side and night-side hemispheres of $\Delta\mathrm{SpT} \simeq 1$, equivalent to $\Delta T \simeq 57$ K with maximum temperature difference of $\simeq 200$ K. **a**, Temperature distribution of the donor's atmosphere as a function of phase. **b**, 1.3 μm water band depth measurements with the best-fit model (solid line) and a model with no irradiation source (dashed line) for comparison. **c**, Timed-resolved J-band photometry (circles) after subtracting the white dwarf and accretion disc contributions. Lines represent same models as panel **b**. Error bars in both panels represent 1σ confidence intervals.

Methods

Mass Determination We performed a radial velocity analysis on the the 1.243 μm and 1.252 μm KI absorption lines formed in the atmosphere of the donor. The trailed spectrum of these features is shown as the inset in Fig. 1. We performed a simultaneous fit to both lines and found the best values for the semi-amplitude $K_2 = 499 \pm 15$ km s^{-1}, the systemic velocity $\gamma = -42 \pm 8$ km s^{-1} and the rotational broadening $v \sin i = 131 \pm 46$ km s^{-1}. When combined with the observed value for the radial velocity semi-amplitude of the WD, $K_1 = 34 \pm 4$ km s^{-1} [25], this allows us to derive a purely dynamical estimate of the mass ratio of the system, $q = M_2/M_1 = K_1/K_2 = 0.068 \pm 0.008$. For this mass ratio, the occurrence of WD eclipses alone sets a firm lower limit on the inclination of $i > 80°$[26]. We can then use the mass function of the secondary, $f(M_2) = (P_{orb}K_1^3)/(2\pi G) = M_1 \sin^3 i/(1+q)^2$, where G is the gravitational constant, to set a purely dynamical 2σ upper limit on the mass of the donor star, $M_2 < 0.071 M_\odot$. We can also use the mass function to obtain a model-independent *estimate* of the donor mass. In any semi-detached compact binary system, there is a unique, single-valued family of $i - q$ pairs that produce a compact object eclipse with a given width[26]. In the case of J1433, the WD eclipse width can be measured directly from published optical light curves[19]. We can then combine the resulting $i - q$ constraint with our spectroscopic mass ratio and the mass function to obtain a robust donor mass estimate that depends only on Kepler's third law and the well-understood geometry of Roche-lobe-filling objects. We find $M_2 = 0.055 \pm 0.008$ M$_\odot$, well below the hydrogen-burning limit.

Water-band ratios and broad-band fluxes. In order to provide the cleanest measurements of the donor at any given phase, we subtracted both white dwarf and accretion disc contributions. The

flux observed from the white dwarf was assumed to be constant in phase, except for phase bins affected by an eclipse. In these, we reduced the flux by the fraction of the bin width during which the white dwarf was occulted. The accretion disc contribution was modelled by fitting a power-law to the optical (3200–5400 Å) waveband (while masking the emission lines) and extrapolating to the NIR. Due to the low S/N of the individual spectra, the telluric removal created artefacts in some regions of the spectra. We identified these regions and masked them before shifting each spectrum to the donor's rest frame. We binned the data into eight orbital phase bins and measured a slightly modified water-band index, defined as $\langle F_{\lambda=1.318\mu m}\rangle/\langle F_{\lambda=1.340\mu m}\rangle$, where the fluxes are averages over a 5 Å window. This index was then calibrated against brown dwarf spectral type templates[11]. Errors were estimated via 500 bootstrap copies of the median flux inside every orbital bin for all the spectra. The broad-band flux modulation was estimated by integrating the donor flux over the J-band (after masking all emission lines) and converting to AB magnitudes.

Day- and night-side temperatures, albedo and intrinsic luminosity. In order to model the orbital-phase-dependent water band ratios and broad-band flux, we constructed a grid of irradiated donor models with ICARUS[23]. Each of these models is characterized by two parameters: the irradiating luminosity absorbed by the donor, and the intrinsic luminosity it would produce in the absence of irradiation. For each parameter pair, we use ICARUS to calculate the resulting temperature distribution across the donor and to predict the observed spectrum at each orbital phase. These calculations assume that all of the irradiating flux absorbed at a given point on the donor's surface is re-emitted locally and neglect any effect of the donor's fast rotation on the temperature distribution (which could affect the atmospheric dynamics[24]). However, the distorted shape of the

Roche-lobe-filling donor, as well as limb- and gravity-darkening, are fully taken into account in these calculations. The absorbed irradiating and intrinsic luminosities are not directly observable, but they respectively determine the day-side and night-side temperatures, which are. We therefore present our results in terms of these temperatures, which we calculate by summing over all day-side surface elements in the model,

$$\langle T_{\rm day} \rangle = \left(\frac{1}{\sigma} \frac{\sum_{j,\rm day} F_{{\rm tot}_j}}{\sum_{j,\rm day} A_j} \right)^{1/4},$$

and all night-side elements,

$$\langle T_{\rm night} \rangle = \left(\frac{1}{\sigma} \frac{\sum_{j,\rm night} F_{{\rm int},j}}{\sum_{j,\rm night} A_j} \right)^{1/4}.$$

Here, $F_{{\rm int},j}$ is the intrinsic flux and is given by

$$F_{{\rm int},j} = A_j \sigma T_{{\rm int},j}^4,$$

where A_j is the area of the surface element, and σ is the Stefan-Boltzmann constant. As a consequence of the distorted shape of the donor, $T_{{\rm int},j}$ – the temperature of each surface element in the absence of irradiation – is not constant. Similarly, the total flux that heats each surface element on the day-side, $F_{{\rm tot},j}$, is given

$$F_{{\rm tot},j} = F_{{\rm int},j} + (1 - A_B) F_{{\rm irr},j},$$

where A_B is the bolometric (Bond) albedo of the donor. $F_{{\rm irr},j}$ is the irradiating flux seen by this element, given by

$$F_{{\rm irr},j} = \frac{4\pi R_{\rm WD}^2 \sigma T_{\rm WD}^4}{4\pi d_j^2} A_{{\rm proj},j}.$$

Here d_j is the distance of every surface element to the white dwarf, $T_{\rm WD}$ is the white dwarf temperature and $A_{{\rm proj},j}$ is the projected surface intercepting the irradiating flux. Since we have good

estimates of the white dwarf temperature and binary parameters, $F_{\mathrm{irr},j}$ is well-constrained observationally. Thus the *absorbed* irradiating flux and the day-side temperature can equivalently be thought of as measures of the albedo. We determine optimal values of $\langle T_{\mathrm{day}} \rangle$, $\langle T_{\mathrm{night}} \rangle$, and A_B by fitting the observed phase-dependent water-band and broad-band fluxes using a Markov-Chain Monte Carlo procedure. The results are shown in the Extended Data Figure 1. We find $\langle T_{\mathrm{night}} \rangle = 2344^{+11}_{-10}$ K and $\langle T_{\mathrm{day}} \rangle = 2401^{+7}_{-7}$ K, where the errors represent the 1σ confidence levels. The corresponding constraints on the albedo and intrinsic donor luminosity are $A_B < 0.54$ (at 2-σ) and $L_{int} = 3.1 \pm 0.1 \times 10^{-4} L_{\odot}$. In all of these models, we adopt a white dwarf temperature of $T_{\mathrm{WD}} = 13200 \pm 200$ K, based on our own analysis of ultraviolet data obtained by GALEX, $i = 84.36^{\circ}$ for the inclination, $d = 226$ pc for the distance, and $P_{orb} = 78.106657$ min for the orbital periods, based on previous eclipse modelling estimates[9]. We also adopt a fixed gravity-darkening coefficient of $\beta = 0.08$[27]. z

Heat Redistribution Across the Terminator. Our geometric reprocessing model assumes that none of the irradiating flux is redistributed from the day-side to the night-side. This model fits the data acceptably, suggesting that redistribution is inefficient in the atmosphere of the donor. In order to estimate this efficiency quantitatively, we need to adopt a specific model for redistribution. Here, we assume that a constant fraction $0 \leq \epsilon \leq 1$ of the irradiating flux that is absorbed at any point on the day-side of the donor is redistributed evenly across the entire surface. Similar models are commonly used in studies of irradiated exo-planets [28]. In the context of this simple model, the difference between the fluxes emerging from the day-side and the night-side is given by

$$\sigma \langle T_{\mathrm{day}} \rangle^4 - \sigma \langle T_{\mathrm{night}} \rangle^4 = \left(\sigma \langle T_{\mathrm{day}} \rangle^4 - \sigma \langle T_{\mathrm{night}} \rangle^4 \right)_{\epsilon=0} - \epsilon (1 - A_B) \frac{\sum_{j,\mathrm{day}} F_{\mathrm{irr}_j} A_j}{\sum_{j,\mathrm{day}} A_j},$$

where $(\sigma\langle T_{\rm day}\rangle^4 - \sigma\langle T_{\rm night}\rangle^4)_{\epsilon=0}$ is the flux difference of the equivalent model without any redistribution. The modelling described in the previous section provides us with a set of set of self-consistent flux differences for models with $\epsilon = 0$. We can therefore transform these to the flux differences predicted for otherwise equivalent models with $\epsilon > 0$. Since our earlier modelling also provides us with estimates of the *observed* day-side and night-side temperatures, we can estimate ϵ by comparing the observationally inferred flux difference to that predicted by our transformed models with $\epsilon > 0$. The results are shown in Extended Figure 2. We find that the efficiency of redistribution is indeed low, $0.1 < \epsilon < 0.4$, with higher values corresponding to lower albedos. The 2 σ upper limit on the redistribution efficiency (for $A_B = 0$) is $\epsilon < 0.54$.

25. Tulloch, S. M., Rodríguez-Gil, P. & Dhillon, V. S. Radial velocity study of the post-period minimum cataclysmic variable SDSSJ143317.78+101123.3 with an electron-multiplying CCD. *Mon. Not. R. Astron. Soc* **397**, L82–L86 (2009).

26. Chanan, G. A., Middleditch, J. & Nelson, J. E. The Geometry of the Eclipse of a Pointlike Star by a Roche-Lobe Companion. *Astrophys. J.* **208**, 512–517 (1976).

27. Lucy, L. B. Gravity-Darkening for Stars with Convective Envelopes. *Zeitschrift fuer Astrophysik* **65**, 89 (1967).

28. Cowan, N. B. & Agol, E. The Statistics of Albedo and Heat Recirculation on Hot Exoplanets. *Astrophys. J.* **729**, 54 (2011).

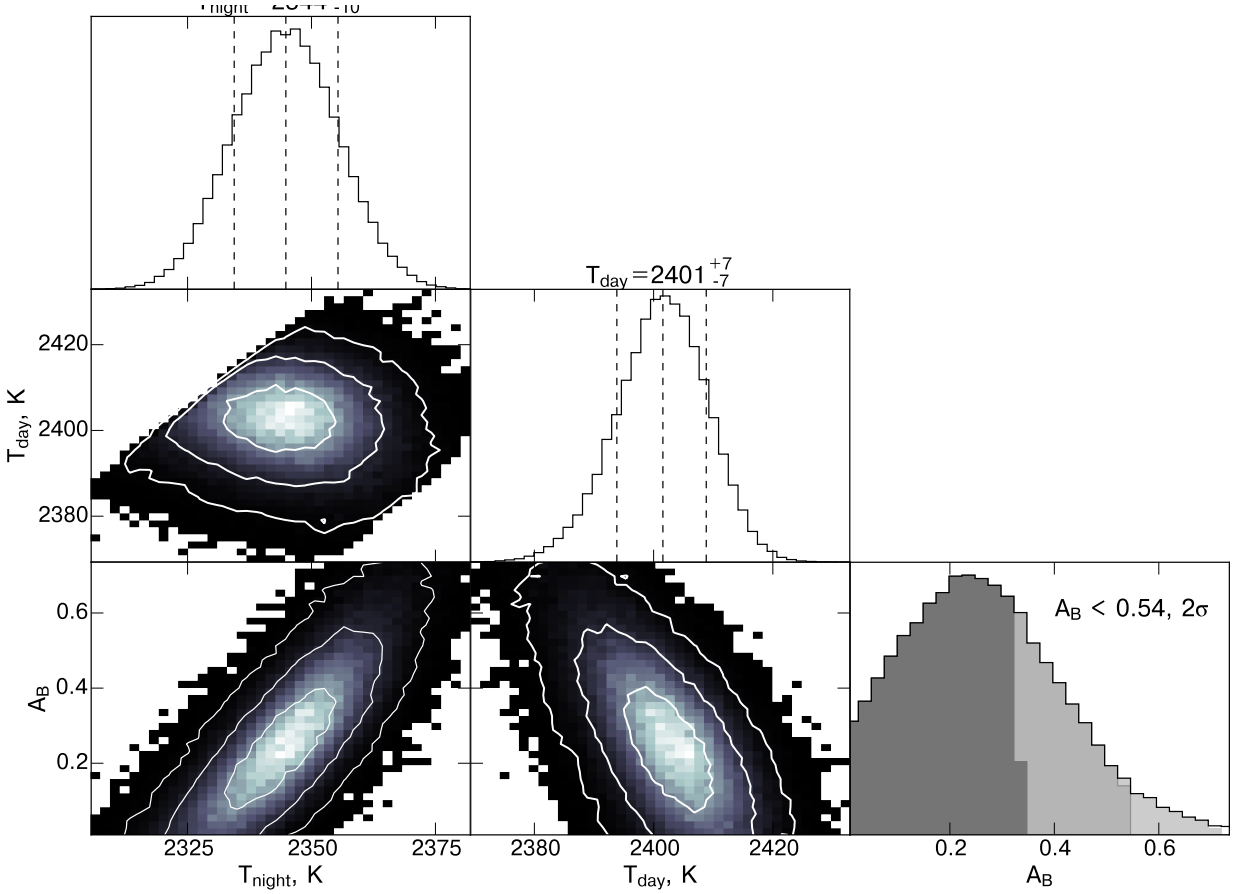

Extended Data Figure 1 | Posterior probability distributions for the irradiation model parameters. Colour scale contours show the joint probability for every combination of parameters. Contours represent the 1, 2 and 3-σ levels. Marginal posterior distributions are shown as histograms with the median and 1-σ marked as dashed lines. The A_B distribution is quoted as a truncated distribution with a 2-σ upper limit.

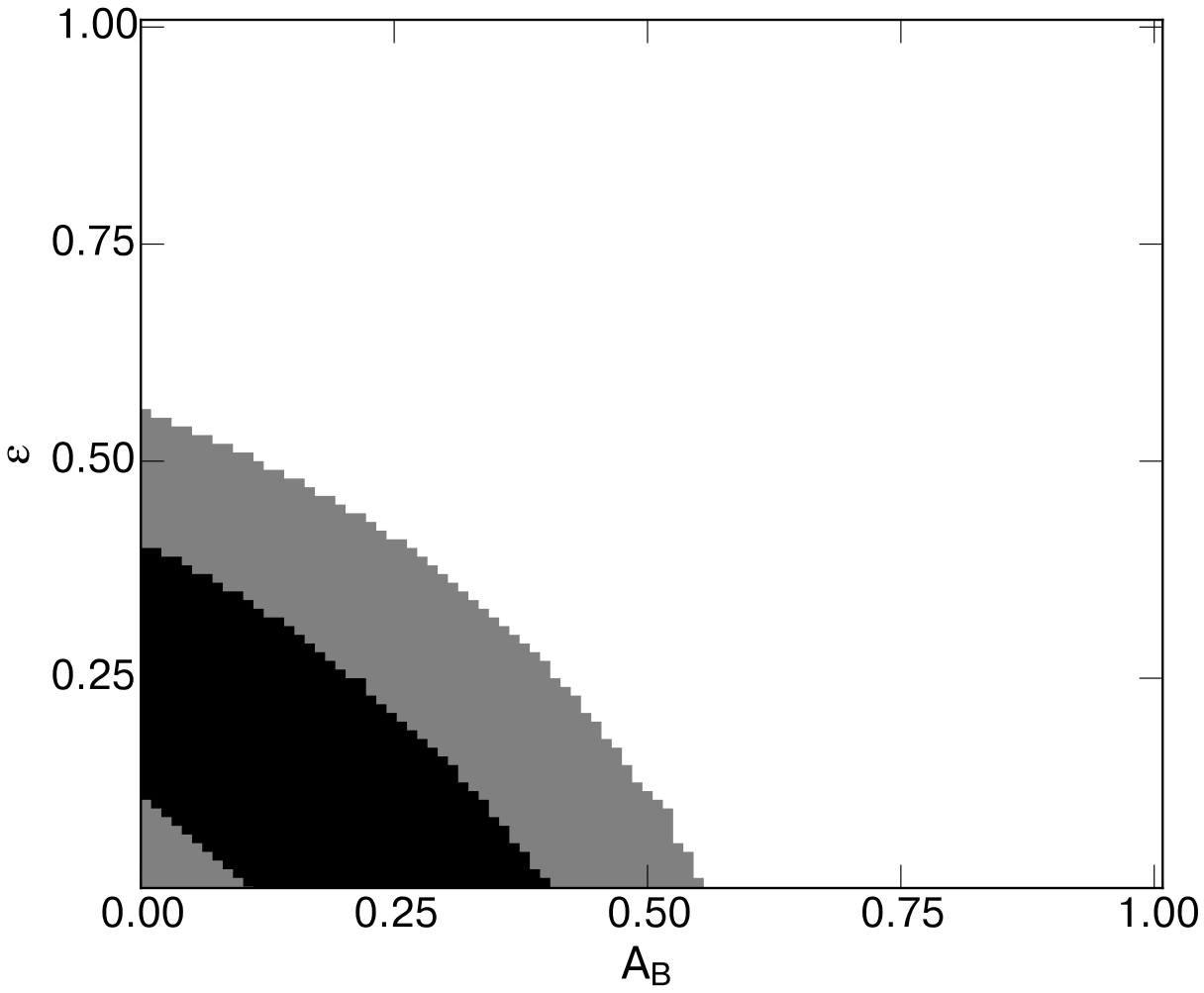

Extended Data Figure 2 | Redistribution efficiency limits for the irradiated sub-stellar donor. Allowed family solutions of redistribution efficiencies as a function of Bond albedo are shown. The black and grey contours represent the 1 and 2-σ confidence levels.